Osmotic Pressure, Correlation Lengths and Viscosity of Pullulan Beyond the Overlap Concentration

Lingzi Meng¹, Rene Iwato², Takaichi Watanabe^{2*}, Carlos G. Lopez^{1*}

 Department of Materials Science and Engineering, The Pennsylvania State University, 80 Pollock Rd, State College, 16802, PA, USA.
 Department of Applied Chemistry, Graduate School of Environmental, Life, Natural Science, and Technology, Okayama University, 3-1-1 Tsushima-naka, Kita-ku, Okayama, 700-8530, Japan.

*Corresponding author(s). E-mail(s): wata-t@okayama-u.ac.jp; cvg5719@psu.edu;

Abstract

We investigate the thermodynamic, scattering, and flow properties of pullulan, a flexible non-ionic polysaccharide in aqueous solution, focusing in semidilute and concentrated solutions. We review dilute solution data for the intrinsic viscosity and radius of gyration and hydrodynamic radius of aqueous pullulan and find the Kuhn length and thermal blob size to be 3 nm and 20 nm, respectively. We establish the scaling laws for static correlation length, specific viscosity, osmotic pressure, and osmotic compressibility across dilute, semidilute, and concentrated regions, finding that the scaling exponents align well with theoretical predictions but the cross-over concentrations obtained from different methods are not consistent. The ratio between the osmotic and Ornstein–Zernike correlation lengths ξ_{Π}/ξ_{OZ} to be approximately 2.5 for aqueous, similar to that observed for polystyrene in a theta solvent. This similarity may arise because the crossover concentration between the semidilute and concentrated regions c^{**} is close to the overlap concentration c^* .

Keywords: Pullulan, Osmotic pressure, Correlation length, Semidilute solutions, Concentrated solutions, Viscosity, SAXS, SANS, DLS

1 Introduction

Pullulan is a linear, water-soluble polysaccharide produced by fermentation of Aureobasidium pullulans. Its repeating unit consists of maltotriose blocks connected by $\alpha(1\rightarrow 6)$ glycosidic linkages, while the glucose residues within each block are linked by $\alpha(1\rightarrow 4)$ bonds. This combination of linkage types leads to high chain flexibility and prevents the formation of extended helices in aqueous solution, though some local curling is known to occur and is reflected in the relatively short z-projected monomer length of 0.3 nm, compared to the longer values of 0.5 nm observed for β -linked polysaccharides.[1-6]

Fig. 1 Monomer structure of pullulan, composed of three glucose units linked by $\alpha(1-4)$ bonds (red lines). Successive monomers along the chain are connected by $\alpha(1-6)$ bonds (blue lines).

Because of its non-toxicity, biodegradability, and film-forming properties, pullulan has become an important biopolymer in industrial and biomedical applications.[7–12] In biomedicine, it serves as a matrix for tissue engineering, drug and gene delivery, and 3D bioprinting.[13–16] Thangavel et al. reported that pullulan accelerates skin tissue regeneration by promoting collagen synthesis,[17] while Laksee et al. developed gold-nanoparticle/pullulan hybrids for targeted drug delivery.[18] Oxidized pullulan sponges have been used for rapid hemostasis,[19] and cationic pullulan derivatives show efficient flocculation of metal oxides such as FeO and TiO₂.[20] In cosmetic and food products, pullulan functions as a biocompatible adhesive and oxygen-barrier material, enabling biodegradable coatings and prebiotic formulations.[13, 14, 21, 22]

In dilute solution, pullulan has been extensively characterized by light and X-ray scattering, ultracentrifugation, viscosimetry, and simulation.[2–5, 23–25] These studies consistently indicate a Kuhn length of approximately 3 nm, smaller than those of β -linked polysaccharides such as cellulose ethers, which typically display $l_K \simeq 10$ -30 nm,[26–30] and comparable to α -linked chains such as amylose.[31] In contrast, much less is known about its structure and thermodynamics in the semidilute and concentrated regimes. Most available work focuses on rheology,[32–37] whereas systematic scattering and osmometry data are largely lacking.

The physical properties of flexible polymers in good and θ solvents are expected to follow universal scaling exponents, with crossovers at the overlap (c^*) and semidilute-to-concentrated (c^{**}) concentrations.[38, 39] Above c^* , excluded-volume interactions become progressively screened, leading to a reduction in chain size that approaches ideal-coil dimensions at $c \simeq c^{**}$. Hydrodynamic interactions are also screened when

 $c > c^*$, producing a transition from Zimm dynamics in dilute solution to Rouse-like dynamics in concentrated solutions and melts.

The present work combines osmometry, small-angle X-ray scattering, and rheological measurements on aqueous pullulan solutions over a wide concentration range to probe their structural and thermodynamic properties. We determine the concentration dependence of osmotic pressure, static correlation length, and viscosity, extract the corresponding scaling exponents, and identify the crossover concentrations separating the dilute, semidilute, and concentrated regimes. The analysis reveals that while the exponents agree with theoretical predictions, the transition from semidilute to concentrated behavior inferred from osmotic pressure occurs at much higher concentrations than that derived from viscosity. In addition, the static correlation length obtained from Ornstein–Zernike analysis does not display a concentrated crossover, and good-solvent scaling is observed throughout the measured range. The ratio between osmotic and scattering correlation lengths, $\xi_{\Pi}/\xi_{OZ} \simeq 2.5$, is similar to that found for polystyrene in θ solvents, suggesting that despite the discrepancies between theory and experiments note above, the screening mechanisms governing flexible polysaccharides in aqueous solutions share similarities with synthetic polymers in organic media.

Table 1 Some physical and commercial properties of pullulan. a typical commercial samples. b in aqueous solution. c This work

Repeating unit molar mass	486 g/mol
M_w	$\simeq 2-3 \times 10^5 \text{ g/mol}^a$
partial specific volume ^b	0.6 mL/g [25]
1 1	2 400 K
Glass transition temperature[32]	≥ 400 K 570 K
Decomposition temperature ^c	0.011
Tensile Strength	30-54 MPa [40]

2 Materials and Methods

Chemicals: The pullulan sample was provided by Hayashibara Co., Ltd (Okayama, Japan). Deionised water with resistivity 18.2 M Ω was obtained from a ELGA Purelab Flex 3 Water Purification System. Spectra-Por dialysis membranes (MWCO = 12-14 kDa) were purchased from WVR. Filters with pore size 0.1 μ m were purchased from CELLTREAT Scientific Products.

Solution preparation: Bacteria were observed in pullulan solutions after several days, especially for higher concentrations. Thus, the deionized water obtained from the ELGA Purelab Flex 3 Water Purification System was filtered using 0.1 μ m PES membrane filters to get rid of bacteria. The plastic vials used to prepare and store solutions were cleaned in advance using filtered deionized water and IPA. Pullulan solutions with specific concentrations were prepared gravimetrically by dissolving the pullulan polymer in filtered deionized water. They were left on the roller for at least one day to dissolve before any measurement.

Dialyzed pullulan was required for osmotic pressure measurement and was obtained using the Spectra-Por dialysis membranes. Around 10 mL 1wt% pullulan solution was dialysed against 5 L deionized water for 2 days. The conductivity of the bath was $\simeq 3.5 \ \mu\text{S/cm}$, which can be assigned to dissolved CO₂ from the air.[41]

Freeze drying: A FreeZone freeze dryer from Labconco Corporation was used. The samples were frozen using liquid nitrogen before loading into the freeze dryer. Kimwipes were used to cover the opening of the centrifuge tubes to prevent the loss of polymer. The freeze-drying process was conducted at around -87.5 degrees °C and 0.95 mbar for around 2 days.

Ultrasonication: A 1800W 2-in-1 Ultrasonic Homogenizer Ultrasonicator Cell Disruptor Mixer from U.S. Solid was used to reduce the molar mass of pullulan. Pullulan solutions with initial concentrations of 1wt% and 5wt% were ultrasonicated for one hour (rested for 1s after every 4s of sonication) under 50% power. The solutions were filtered using filter paper and freeze-dried after ultrasonication.

Small angle x-ray scattering (SAXS): SAXS measurements were carried out at the BL40B2 instrument of the Spring-8 synchrotron (Hyogo, Japan). The sample to detector distances used were 1.2 m and 2 m and the x-ray energy was set to 12.2 keV. Samples were loaded onto capillaries with diameter $\simeq 2$ mm and measured for 20-60s. Transmission measurements were simultaneously recorded. Capillary thicknesses at the position approximately corresponding to the incident beam were recorded with a caliper. The scattering intensity of water was measured for each different setup and included in table S1.

Small angle neutron scattering (SANS): The SANS-U instrument at the JRR-3 facility in Tokai, Japan was used to record the scattering patterns of pullulan solutions in D_2O . Samples were loaded into quartz cells of 2 mm path-length. The sample-to-detector distances were set to 1m and 4m, and the wavelength was 7 Å. Data were reduced according to standard procedures and calibrated onto an absolute scale using the direct beam flux. The D_2O measurement gave an intensity of $\simeq 0.035 \text{cm}^{-1}$, in agreement with other reports.[42]

Dynamic light scattering (DLS): DLS experiments were carried out using a CGS-3000XX (ALV GmBH, Germany) equipped with two detectors at the same angle operating in cross-correlation mode. The light source is a $\lambda = 633$ He-Ne laser. Samples were loaded onto 1 cm diameter disposable cylindrical cuvettes made of borosilitcate. minutes. The samples were filtered through syringe filters with a pore size of 0.1 and 0.2 μ m (PES, CELLTREAT Scientific Products).

Capillary viscosimetry: Ubbelohde viscometers from CANNON Instrument Company (Viscometer constants K=0.0018902, 0.0019974, 0.002186 and 0.007439 mm²/s²) were used to measure the shear viscosities below the overlap concentration and determine the intrinsic viscosity. The dynamic viscosity was calculated by multiplying the flow time with the solution density and a constant, which was calibrated by a standard solution with known dynamic viscosity.

Spinning ball viscosimetry: An EMS-1000s viscometer (KEM Instruments, Kyoto, Japan) was used to measure the viscosity of pullulan solutions at different concentrations. The instrument operates by suspending an aluminium ball on a vial containing

the sample. Two magnets rotate around the ball and the rotation speed is measured by a camera.

Rotational Rheology: A controlled-stress Kinexus-ultra rheometer (Netzch) was used with a cone-plate geometry (angle $=1^{\circ}$, diameter =40 mm). The temperature was set to 25 °C using a Peltier system. A solvent trap was employed to reduce evaporation.

Freeze Point Depression (FDP) Osmometry: An Osmotech XT freeze point depression osmometer (Advanced Instruments, US) was used to measure the osmotic pressure of pullulan solutions in water. The instrument is designed to handle viscous samples, which are usually problematic for FPD osmometers. Selected solutions were also measured on a 3320 osmometer (Advanced Instruments), but this instrument did not yield stable results despite working well for solutions of simple salts. Both osmometers measure the freezing point by supercooling the sample, inducing crystallisation via mechanical agitation and recording the equilibrium temperature as the sample heats up to the melting point. The result is displayed in terms of osmolality (C_{Osm}) , where $C_{Osm} = 1.86\Delta T_f$ is assumed, with ΔT_f the change in freezing point of the sample with respect to pure water and 1.86 Kkg/mol is the cryoscopic constant of water.

The osmotic pressure is calculated from the freeze point depression (ΔT [K]) as:

$$\Pi = RT \frac{\Delta T}{1.86}$$

where T = 273.15 K and R is the gas constant.

Size-exclusion chromatography (aqueous): Size Exclusion Chromatography with multi-angle light scattering (SEC-MALS) experiments were carried out using an Agilent 1260 Infinity II HPLC system equipped with an autosampler. Wyatt Technology DAWN MALS, Wyatt Optilab refractive index detector and Agilent UV detector were used for analyzing the molar mass of peaks that eluted from the column and were normalized and aligned using standard BSA. The Wyatt silica-based 300 Angstrom SEC column was used. The system was equilibrated with 0.01 M NaCl buffer solution for five hours in advance. UV was set to 280 nm and temperature was set to 25°C. 100 μ L of 2 mg/mL pullulan solution was injected at a flow rate of 0.5 mL/min with a chromatogram run time of 40 min. The concentration source used was RI. the ASTRA software (Wyatt) Version 8.2.2 was used for data analysis.

Size-exclusion chromatography (DMF): The molar mass distribution of pullulan was determined using a gel permeation chromatography (Prominence-GPC system, Shimadzu, Japan), equipped with a refractive index detector and columns (TSK guard column Super H-H, TSKgel Super HM-H, and TSKgel Super H2000, TOSOH, Japan). DMF (GPC grade, purity 99.7%, FUJIFILM Wako Pure Chemical Corporation, Japan) was used as the eluent at a flow rate of 1.0 mL min⁻¹. The polystyrene standard (TSK standard polystyrene, Tosoh, Japan) was used to make a calibration line

Thermogravimetric Analysis The mass loss of pullulan upon heating was evaluated using a thermogravimetric/ differential thermal analyzer (TG, DTG-60, Shimadzu, Japan). Approximately 10 mg of the sample was placed on an alumina open pan on

the TG stage, and the profile was recorded from room temperature to 500 $^{\circ}$ C at a heating rate of 10 $^{\circ}$ C min⁻¹ in a nitrogen atmosphere.

All numerical data are included in the supporting information.

3 Results and Data Fitting

Sample preparation, storage, purification and characterisation

Solutions of pullulan in water were found to grow bacteria over time. This effect was more pronounced for solutions of higher concentrations. Bacterial growth could be slowed down by keeping samples refrigerated at 4 o C and by using DI water filtered through 0.1 μ m filters.

Experiments on solutions made with the as received polymer were found to display abnormally high osmotic pressures. This was interpreted as arising due to the presence of low molecular weight non-volatile compounds in the polymer powder. Dialysis against DI water was carried out and the polymer was freeze dried. Solutions made from the dialysed polymer gave lower osmotic pressures which were found to compatible with data from literature studies employing membrane osmometry, see figure 8 and related discussion. [43] If we assume the impurities are monosaccharides ($M \simeq 180$ g/mol), the difference in osmotic pressures between the dialysed and non-dialysed samples would correspond to $\simeq 2$ wt% of the polymer powder. The osmometry results presented below are for purified pullulan. The viscosity of solutions for $c \simeq 5-10$ wt% were found to the same within experimental error for the solutions prepared from dialysed and as received polymer, as expected given the low fraction of oligosaccharides. The SAXS curves of dialysed and non-dialysed samples also did not show any differences.

Table 2 Molar mass averages from size-exclusion chromatography and intrinsic viscosity. All values are in kg/mol.

M [kg/mol]	M_n	M_w	M_z	M_{z+1}
SEC (DMF)	241	297	353	409
SEC (Aqueous)	265	290	315	340
MHS		268		
Average	253	285	334	375

Table 2 lists the molar mass averages obtained from size-exclusion chromatography. Data obtained in DMF and in aqueous buffer show good agreement. An estimate for the weight-averaged molar mass was also obtained from the intrinsic viscosity, using the MHS relation discussed below. This gives a value which agrees well with the SEC measurements.

The mass of pullulan as a function of temperature is plotted in the supporting information. A plateau in the weight for temperatures between 150 and 250 °C was use to estimate the water content as 7.3 wt%. Sample concentrations are adjusted based on this water content.

3.1 SAXS and SANS

The scattering signal of the sample $I(q)_s$ was obtained by subtracting the signal of the capillary cell from that of the cell+sample:

$$I(q)_s = \frac{N(q)_{s+c}}{tT_{s+c}} - \frac{N(q)_c}{tT_c}$$
 (1)

Where N(q) represents the count rate at a specific scattering wave vector q, t is the thickness of the capillary cell and T is the transmission. The subscripts s and c represent the sample and capillary cell respectively. For a series of samples were measured at 1 and 2m sample-to-detector distances, we stitched curves together by multiplying the 1m data by a constant.

The scattering signal in absolute units (cm⁻¹) $I(q)_s$ was then obtained by multiplying the ratio of the experimental scattering signal of water and the known scattering of water $(1.632 \times 10^{-2} \text{ cm}^{-1}).[44]$ Table S1 shows the experimental scattering signal of water for the different setups used. The scattering signal for a neutral polymer can

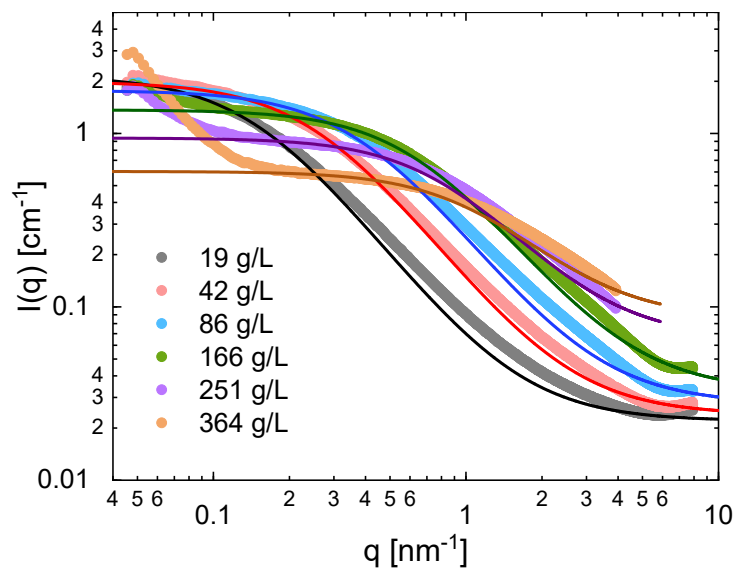


Fig. 2 The scattering intensities I(q) for samples with different concentrations are plotted as a function of scattering wave vector q. Both raw data (points) and OZ fitting (lines) are shown in this figure.

be fitted using Ornstein-Zernike (OZ) function:

$$I(q) = \frac{I(0)}{1 + (q\xi_{OZ})^2} + I_B \tag{2}$$

where I(0) is the scattering intensity at zero-angle, ξ_{OZ} the correlation length and I_B a background term that accounts for q-independent scattering.

After subtraction, normalization, and stitching, $1/[I(q) - I_B]$ was plotted as a function of q^2 and is known as the Debye plot. Based on the OZ function, the Debye plot can be fitted within the range of $q\xi < 1$ by a straight line with a slope of $\xi^2/I(0)$ and an intercept of 1/I(0). Examples fits to the OZ function are shown in figure 2.

SANS data displayed stronger low-q upturns than the SAXS measurements, which made the accurate determination of the correlation length impossible. Filtration through 0.1 or 0.2 μ m membranes reduced the upturn but not sufficiently to allow for reliable fitting. SANS curves for eight different concentrations are included in the supporting information for reference.

3.2 Osmometry

Table 3 compiles the osmotic pressure data obtained for pullulan solutions in DI water. Preliminary measurements for the freeze point depression showed that the 'as-received' pullulan displayed abnormally high osmotic pressure. Solutions of the polymer purified by dialysis yielded more reasonable results, suggesting the presence of a small fraction of oligomers in the as-received powder, see the supporting information for a comparison of the dialysed and undialysed data. The high viscosity of concentrated samples made sample loading into the FDP osmometer difficult. Therefore, the lower molar mass polymer obtained by ultrasonic degradation was used for some high concentration samples. The values for the two polymers agree well.

Table 3 Osmotic pressure data for dialysed pullulan solutions. Freezing point depression data are measured on the OsmotechXT (OXT) a ultrasonicated sample

c [g/L]	Π_{FPD} [kPa]	c [g/L]	Π_{FPD} [kPa]
53.86	4.54	182.36	133.93
69.25	11.35	196.60	154.36
92.02	27.24	145.35	59.02^{-a}
115.05	52.21	158.63	88.53^{a}
128.08	68.10	183.37	111.23^{a}
154.19	70.37	211.04	199.76^{-a}

3.3 Viscosimetry and Rheology

The intrinsic viscosity $[\eta]$ of the pullulan sample was determined from capillary viscosimetry experiments. The intercepts of both Huggins and Kraemer's plots, shown in figure S1 are similar and give an average intrinsic viscosity of 0.0826 L/g. The molar mass estimated from the $[\eta] - M_w$ relationship is $2.68 \times 10^5 \text{g/mol}$, in good agreement with the results of SEC in both aqueous and DMF media. The Huggins (k_H) and Kraemer's (k_K) coefficients are estimated to be 0.368 and -0.146, which satisfy the expected relation $k_H - k_K \simeq 0.5$. Our value of k_H is consistent with literature results, plotted in figure S2, which show $k_H \simeq 0.4$ for $M_w \gtrsim 50 \text{ kg/mol}$.

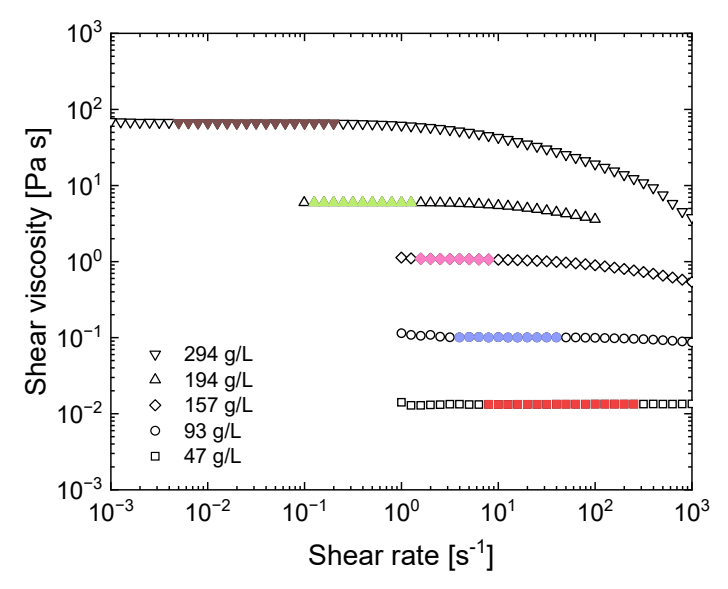


Fig. 3 Viscosity vs. shear rate curves for pullulan solutions in DI water. Full symbols are data used to calculate the Newtonian viscosity.

The shear viscosity of pullulan samples with different concentrations measured using Kinexus rheometer are plotted as a function of shear rate in figure 3. The average of the value in the Newtonian region is taken as an estimation of the zero shear-rate viscosity. These values are tabulated for all concentrations measured in the supporting information.

3.4 Dynamic light scattering

The field correlation functions were fitted using a modified cumulant expansion:

$$g_1(q,\tau) = e^{-\Gamma\tau} \left(1 + \frac{\mu_2 \tau^2}{2} \right)$$
 (3)

where τ is the correlation time, Γ is the inverse relaxation time or first cumulant, and μ_2 is the second cumulant, which is related to the variance of the distribution of relaxation times.

Equation 3 was fitted to the measured intensity correlation function using the Siegert relation to obtain the best fit values of Γ and μ_2 , example fits are shown in fig S3. The apparent diffusion coefficient (D_{app}) is obtained by taking the average value Γ/q^2 over the entire q-range measures, see figure S4. The translational diffusion coefficient (D_0) at infinite dilution is then calculated by linearly extrapolating the apparent diffusion coefficient to zero concentration:

$$D_{app}(c) = D_0(1 + k_D c)$$

where k_D is the diffusion virial coefficient. The plot of D_{app} against concentration is shown in fig. S5. We obtain $D_0 = 1.47 \times 10^{-11}$ m²/s, corresponding to $R_H = 16.7$ nm, $k_D = 0.024$ L/g.

The dimensionless ratio $(6\pi)^{-1}\sqrt[3]{[\eta]M_w/(N_AR_H^3)}$ takes a value of 0.106, in good agreement with values observed for many polymer systems. [45] This confirms the validity of our determination of M_w , R_H and $[\eta]$.

4 Discussion

Throughout this section, we use the term monomer to refer to a glucose unit in the pullulan chain. Strictly speaking, the monomer of pullulan corresponds to the maltriose unit shown in figure 1, however, we find that using the glucose unit as our reference allows for easier comparison with other polysaccharides. Degrees of polymerisation are expressed as N, the number of glucose units on the chain or N_K , the number of Kuhn segments on the chain.

4.1 Dilute solution properties

We compiled intrinsic viscosity, radius of gyration and diffusion coefficient data from refs. [2, 23–25, 35, 46–51]. The intrinsic viscosity data reported in these references were measured using capillary viscometers. Capillary viscometers offer high precision, but for high molar mass polymers, the measured data do not always correspond to the zero shear-rate limit. According to the theory of Fixman[52], the intrinsic viscosity can be expressed as a function of the reduced shear rate $K_{\eta}\dot{\gamma}$, where:

$$K_{\eta} = \frac{1.7\eta_s[\eta]M_w}{RT}$$

When $K_{\eta}\dot{\gamma} \lesssim 1$, the intrinsic viscosity corresponds to the zero-shear rate value. For $K_{\eta}\dot{\gamma} \gtrsim 1$, $[\eta]$ decreases with increasing shear rate, see refs. [45, 53, 54] for experimental data supporting this.

The range of intrinsic viscosities reported in the literature for pullulan extends up to $\simeq 338$ mL/g, with the upper limit corresponding to the 2.56×10^6 g/mol sample reported by Kato el al[23]. We estimated the shear rate applied by their capillary viscometer to be around 1400 s^{-1} based on the efflux time for water reported and assuming a capillary length of 13 cm. For their highest molar mass sample, this corresponds to $K_\eta\dot{\gamma}\simeq 0.74$, so that modest shear thinning is expected.

Figure 4a shows a Burchard-Stocymeyer-Fixman plot for pullulan, using intrinsic viscosity data from refs. [23–25, 35, 46, 47, 50]. A linear function was fitted to data with $M_w < 10^6$ g/mol, giving an intercept of $[\eta]/M_w^{1/2} = 0.1017$ mL $(\text{mol/g}^3)^{1/2}$ which corresponds to the intrinsic viscosity of chains unperturbed by excluded volume. For $M_w \gtrsim 10^6$ g/mol, the plot deviates from linearity. This is expected given that the large N limit for chains in good solvent is $[\eta] \propto N^{0.784}$. Additionally, the reported values in for this range of molar masses may not correspond to the zero shear rate limit, as discussed above.

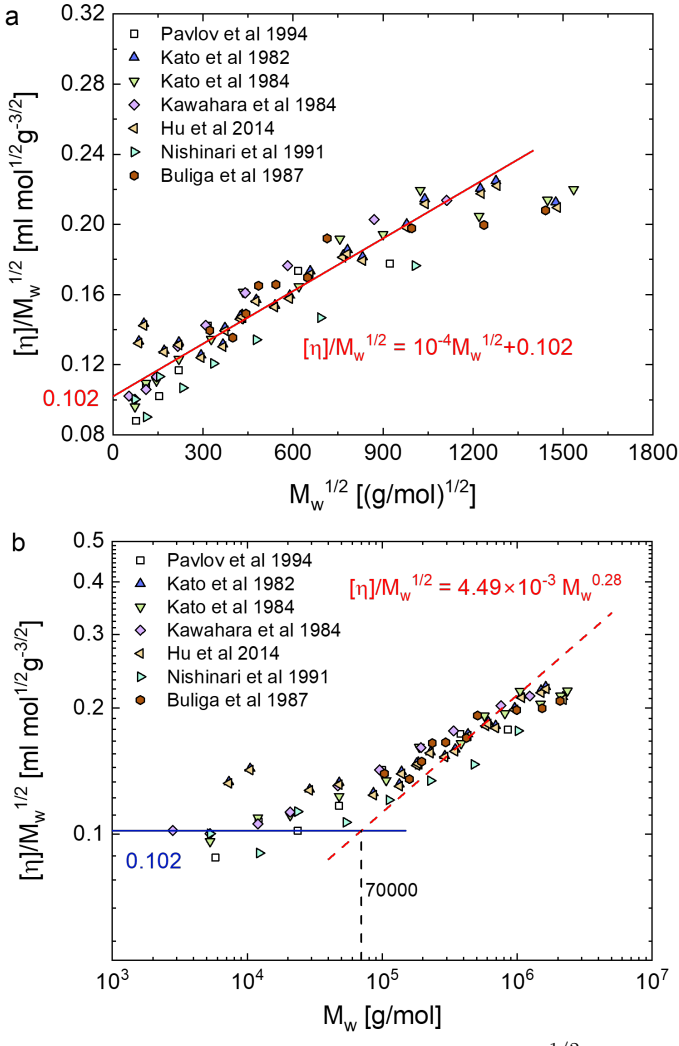


Fig. 4 (a) Burchard-Stockmeyer-Fixman plot. The value of $[\eta]/M_w^{1/2}$ for unperturbed chains is determined by the intercept of the fitting curve of the linear region and y-axis. The red line is a best fit to the data with $M_w < 10^6$, see the text for an explanation. The data by Stankovic et al are excluded from the fit. (b) $[\eta]/M_w^{1/2}$ plotted as a function of weight-average molar mass. The value of $[\eta]/M_w^{1/2}$ for unperturbed chains (blue line) is taken from the intercept of part a. The red dashed line is a fit to the theoretical scaling of chains with the excluded volume. The cross-over between these two regimes allows the molar mass in a thermal blob $M_T \simeq 70000$ g/mol to be estimated. Data are from refs. [23–25, 35, 46, 47, 50].

Having determined the unperturbed intrinsic viscosity of pullulan chains, we next evaluate the properties of the thermal blob, which is the lengthscale at which chains become large enough to be perturbed by excluded volume. [38] Figure 4b plots $[\eta]/M_w^{1/2}$ as a function of molecular weight M_w . The cross-over between the $[\eta]/M_w^{1/2} \propto M_w^0$ scaling and $[\eta]/M_w^{1/2} \propto M_w^{0.284}$, corresponding to the ideal and excluded volume limits

of Zimm chains respectively, is used to estimate the mass of the thermal blob, which is around $M_T \simeq 70,000$ g/mol or $g_T \simeq 432$ monomers.

Figure 5 plots $R_{G,z}$ as a function of the z-averaged molar mass M_z . The data display too much scatter to accurately determine the cross-over between ideal $(R_G \propto M^0)$ and expanded $(R_G \propto M_w^{0.59})$ chains. Therefore, we use the value of $M_T = 70$ kg/mol and fit the data to:

$$R_G = K_\theta M_w^{1/2} \times \begin{cases} 1 & M_w \ll M_T \\ (M_w/M_T)^{0.09} & M_w \gg M_T \end{cases}$$
 (4)

Figure 5 shows a fit Eq. 4, with only K_{θ} as a free parameter, which is found to be 0.03 nm g^{-1/2}mol^{1/2}. This value of K_{θ} can be used to calculate the Kuhn length of pullulan as:

$$l_K = \frac{6K_\theta^2 M_0}{b} \tag{5}$$

where b=0.34 nm is the effective z-projected monomer length, calculated using the value of $M_L=470$ g/mol/nm reported in ref. 2. The value of the Kuhn length obtained is $l_K=2.57$ nm, calculated using equation 5, corresponding to $n_K=l_K/b=7$ monomers per Kuhn segment. The end-to-end distance of the thermal blob ξ_T was calculated as $\xi_T=l_k(g_T/n_K)^{1/2}\simeq 20.4$ nm.

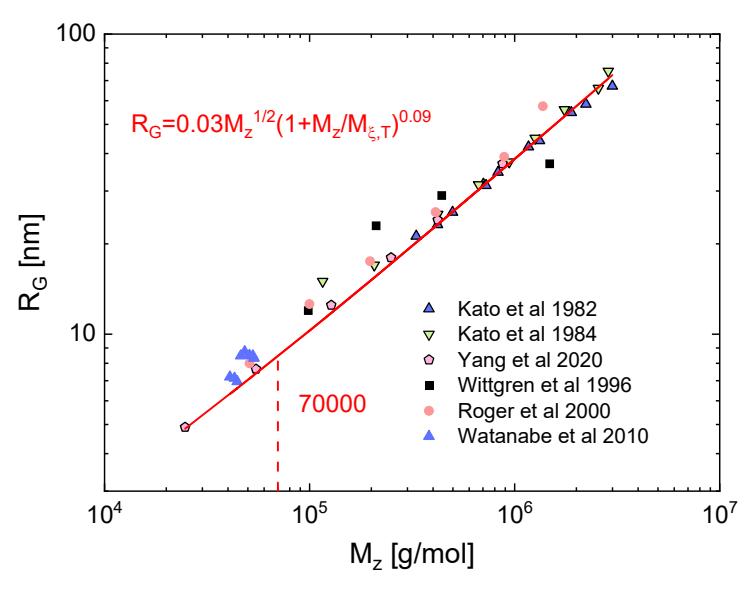


Fig. 5 R_G was plotted as a function of z-average molar mass of pullulan M_z . The size of a thermal blob and the number of monomers in a thermal blob can be calculated based on the cross-over of the scaling laws. Data are from refs. [2, 23, 47–49, 51].

Alternatively, the molar mass dependence of R_G can be described using the worm-like chain model. The unperturbed radius of gyration of a worm-like chain is given

by:

$$R_{G,\theta} = \frac{l_K b N}{6} - \frac{l_K^2}{4} + \frac{l_K^3}{4bN} - \frac{l_K^2}{8b^2 N^2} (1 - e^{2bN/l_K})$$
 (6)

Several approaches exist to take into account the influence of the excluded volume. In the Domb-Barrett approach, the expansion factor α_R , where $R_G = \alpha_R R_{G,\theta}$, is given by:

$$\alpha_S = \left[1 + 10\tilde{z} + \left(\frac{70\pi}{9} + \frac{10}{3}\right)\tilde{z}^2 + 8\pi^{3/2}\tilde{z}^3\right]^{1/15} (0.933 + 0.067e^{-0.85\tilde{z} - 1.39\tilde{z}^2}) \tag{7}$$

with $\tilde{z} = \frac{3}{4}K(Nb/l_K)$. When chains contain six or more Kuhn segments, $K(Nb/l_K) = \frac{4}{3} - 2.711/\sqrt{Nb/l_K} + 7/6Nb/l_K$. The excluded volume parameter is:

$$z = \left(\frac{3}{2\pi}\right)^{3/2} \left(\frac{B}{l_K}\right) \left(\frac{Nb}{l_K}\right)^{1/2} \tag{8}$$

where B is the *excluded volume strength*. If the chain is modelled as a hard-core cylinder, B is given by:

$$B = \pi r_C$$

where r_C is the cross-sectional radius of the chains.

Fitting equations 6-8 to the R_G data for pullulan, shown in figure 6a gives $l_K=3.3$ nm and B=0.2 nm. The value for the Kuhn length is $\simeq 20\%$ larger than the one obtained from the scaling analysis above. The best-fit value of B corresponds to $r_C\simeq 0.6$ Å, which is considerably lower than the cross-sectional diameter of polysaccharides, which is typically around a few Angstroms[6, 55] and indicates that water is a good solvent for pullulan far from the athermal limit. The R_H data compiled from refs. [23, 25, 46, 51, 56–58] and this work are plotted in figure 6b. The Yamakawa and Fujii model was used to calculate the hydrodynamic radius of the unperturbed worm-like chain $(R_{H,\theta})$, see Eq. 47 of ref. [59], shown by the red line. The expansion factor for the hydrodynamic radius was calculated using:[60, 61]

$$\alpha_H = \frac{0.88(1 + 5.93\tilde{z} + 3.59\tilde{z}^2)^{0.1}}{1 - 0.12\alpha_S^{-0.43}} \tag{9}$$

The R_H data are too scattered to allow for the accurate determination of l_K and B and we therefore use the values extracted from the fit to the R_G data. The calculated values for $R_H = \alpha_H R_{H,\theta}$ are shown by the black line in figure 6b and seen to agree well with the data.

A separate estimate for the Kuhn length can be obtained from the value of $[\eta]/M_w^{1/2}$ of unperturbed chains:

$$\frac{[\eta]}{M_w^{1/2}} = \frac{\Phi_0}{N_A} \left(\frac{l_K b}{6M_0}\right)^{3/2} \tag{10}$$

where $\Phi_0=6$ for flexible polymers in the ta solvent is used.[45] This method yields $l_K=2.6$ nm, in good agreement with the estimate for the Kuhn segment based on R_G data. Our estimates for the Kuhn segment are close to the values of $l_K\simeq 3-3.2$

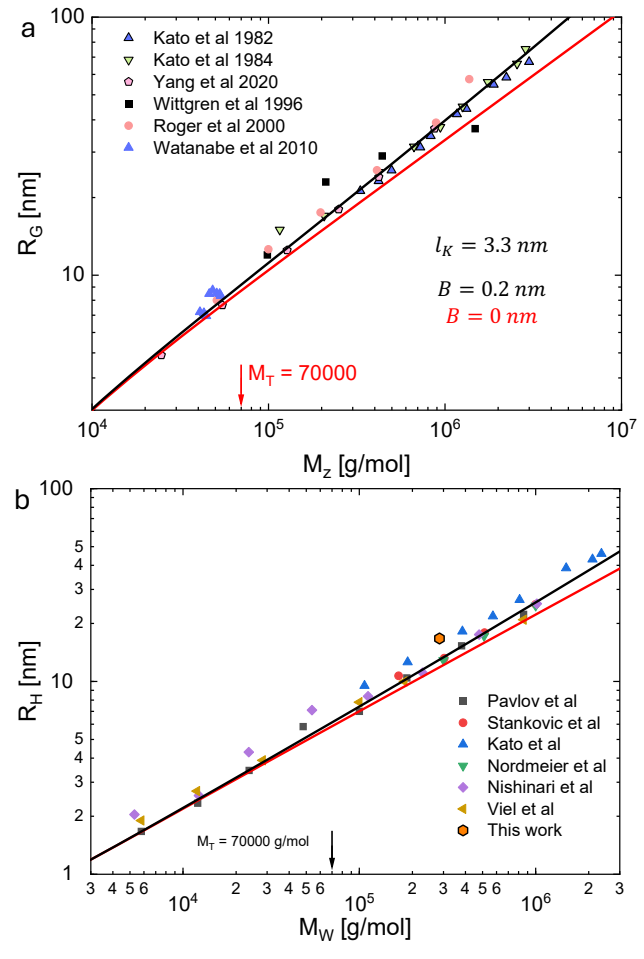


Fig. 6 R_G (top) and R_H bottom, plotted as a function of M_z and M_w respectively. The R_G data are from the same references as in figure 5. R_H data are from this work and refs. [23, 25, 46, 51, 56–58]. Red lines are worm-like chain model without excluded volume (B = 0) and black lines are with excluded volume (B = 0.2 nm).

nm obtained by Yang and Sato[2] by fitting the worm-like chain model to SAXS data of dilute solutions of pullulan.

Second virial coefficient data [2, 23–25, 47, 50, 57] are compiled in figures S10-S11. These show that the interpenetration function takes a value of $\psi = 0.20 \pm 0.02$ in the long chain limit, in line with results for other flexible polymers.

4.2 Semidilute and concentrated solutions

The specific viscosity of pullulan solutions is plotted as a function of concentration in figure 7. Measurements made with the cone-plate geometry on the Kinexus rheometer agree with the capillary viscometer and EMS data. From this we conclude that surface tension effects from the air-water interface [62, 63] do not influence the cone-plate

results. The viscosity data for the dialysed and non-dialysed samples agree within experimental error as expected.

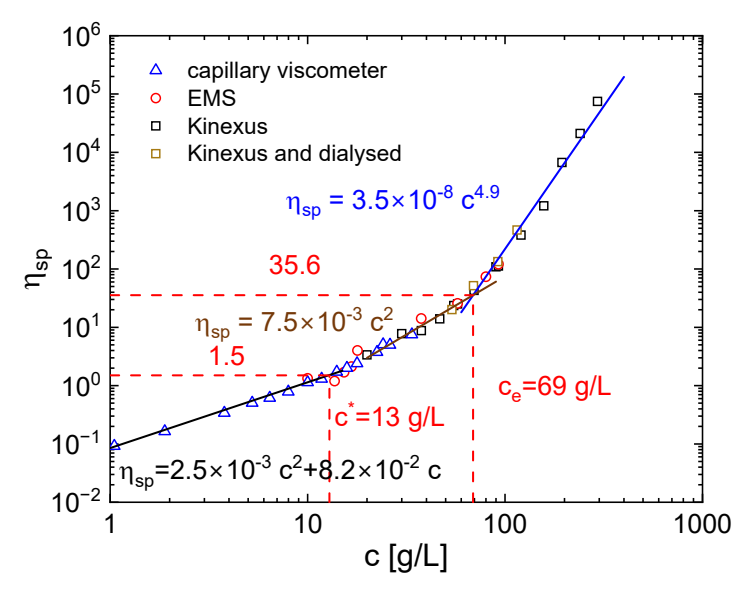


Fig. 7 Specific viscosity η_{sp} plotted as a function of concentration for pullulan in DI water. The overlap concentration is $c^* = [\eta]^{-1}$ and the entanglement concentration c_e is estimated from the onset of the $\eta_{sp} \sim c^{4.9}$ regime.

As discussed above, the specific viscosity can be fitted to Huggins and Kraemer's equations in the dilute region $(c < c^*)$. In the semidilute non-entangled region $(c^* < c < c^{**})$, where c^{**} is the cross-over to the concentrated regime), the specific viscosity is expected to follow the scaling law for good solvents:

$$\eta_{sp}(c) \simeq \eta_{sp}(c^*)(c[\eta])^{1.3}$$
(11)

In the concentrated regime $(c > c^{**})$, the scaling theory predicts:

$$\eta_{sp}(c) \simeq \eta_{sp}(c^*)(c^{**}[\eta])^{1.3}(c/c^{**})^2$$
(12)

The width of the semidilute regime is predicted to be $c^{**}/c^* \simeq 0.044 \times (M_w/M_T)^{0.5} M_w^{0.28} \simeq 3$. For our polymer, this corresponds to $c^{**} \simeq 40$ g/L. The viscosity data instead suggest a crossover to the concentrated regime at $c \simeq 20$ g/L.

Above c^{**} chains should reach their ideal dimensions and behave as in a θ solvent. The Colby-Rubinstein two-parameter scaling for entangled solutions predicts: [64, 65]

$$\eta_{sp} \simeq \eta_{sp}(c_e) \left(\frac{c}{c_e}\right)^{4.9}$$
(13)

Forcing the exponent of 4.9 to our data gives the entanglement concentration as $\simeq 70$ g/L, corresponding to $c_e[\eta] \simeq 5.3$. This value is significantly smaller than the usual

 $c_e[\eta] \simeq 10$ observed for solutions of flexible polymers[38, 66] and is consistent with typical values for semiflexible polysaccharides.[27, 30] For comparison, Hasegawa et al find an exponent of $\eta_{sp} \propto c^6$ for $c > c_e$ and $c_e[\eta] \simeq 9$.[33]

4.3 Osmotic pressure

The water activity (a_w) , relative humidity (RH) and partial vapour pressure data (p^*) data reported in refs. [67, 68] were converted to osmotic pressure data using:

$$\Pi = -\frac{RT}{V_{H_2O}} ln(X)$$

where V_{H_2O} is the partial molar volume of water (18 cm³/mol) and $X = a_w, RH, p^*$. These data are combined with the membrane osmometry data reported by Ayyad[69] and Wang et al [70] as well as the FDP and VPO data measured in this study, which are listed in table 3. The results are shown in figure 8a. The scaling predictions for the semidilute ($\Pi \propto c^{2.25}$) and concentrated ($\Pi \propto c^3$) regimes are shown by the blue and red lines respectively. The crossover between these two regimes is difficult to determine accurately given the scatter in the data, but it appears to be in the vicinity of 100 g/L. A better estimate for this cross-over can be obtained from osmotic compressibility data

The zero-angle scattering intensity is related to the osmotic compressibility of a polymer solution as:

$$I(0) = \overline{K}k_B T c \frac{dc}{d\Pi} \tag{14}$$

where \overline{K} is a contrast factor which for SAXS depends on the electron density of the solvent and solute:

$$\overline{K} = \Delta \rho^2 = \left[(\rho - \rho_s \overline{\nu}) r_o \right]^2$$

where $\Delta \rho$ is the difference between the scattering length per unit volume of pullulan and that of the aqueous solvent. $\rho = 3.2 \times 10^{23} g^{-1}$ and $\rho_s = 3.34 \times 10^{23} \ {\rm cm^{-3}}$ are the number of electrons per mass of dry pullulan and that per volume of the aqueous solvent. $\overline{\nu}$ is the partial specific volume of pullulan as shown in table 1. r_0 is the scattering length of an electron and is around $2.82 \times 10^{-13} \ {\rm cm}$ [71, 72]. \overline{K} is estimated as $1.14 \times 10^{21} \ {\rm cm^2/g^2}$ for pullulan in water.

The power-laws for the osmotic pressure discussed above correspond to a scaling of the osmotic compressibility $cdc/d\Pi$ with concentration of $c^{-0.25}$ and c^{-1} in the semidilute and concentrated regions respectively.

Figure 8b plots $c\frac{dc}{d\Pi}$ as a function of concentration. The data are from the SLS results by Wang et al and SAXS results from this study.[73] The combined data show a clear transition between the semidilute and concentrated exponents at $c \simeq 140$ g/L. This is an order of magnitude higher than the value of c^{**} obtained from viscosity. The two estimates are clearly incompatible and the difference cannot be assigned to experimental error. The reason for this is not understood at present.

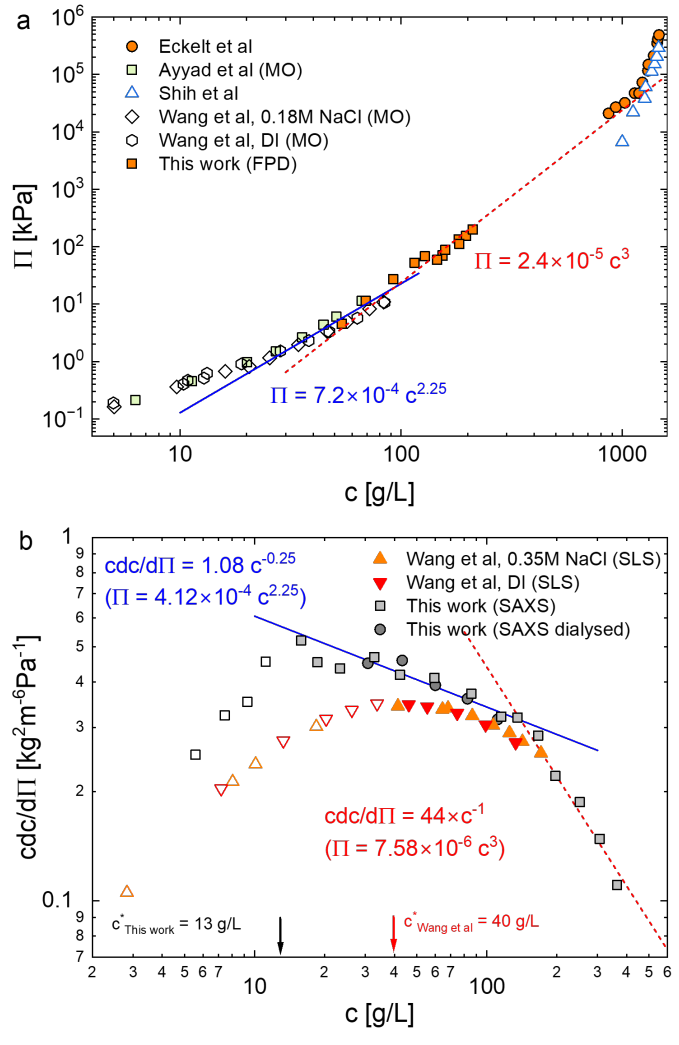


Fig. 8 (a) Osmotic pressure Π is plotted as a function of concentration. Data from this work are measured using FPD osmometry, Ayyad et al and Wang et al's data are measured by membrane osmometry and Eckelt et al and Shih et al are measured by vapour sorption. (b) The osmotic compressibility $cdc/d\Pi$ is plotted as a function of concentration. The hollow symbols represent samples in dilute region, while points in semidilute region are labeled as filled symbols. The values in brackets are the $\Pi-c$ power laws required to get the best-fit $dc/d\Pi$. These deviate somewhat from the ones obtained from direct measurements of the osmotic pressure. Data are from this work and refs. [67–70, 70].

4.4 Screening lengths

The static (Ornstein-Zernike) correlation length obtained from SAXS data is plotted as a function of concentration in figure 9a. In the dilute region, an approximately c-independent value of $\xi \simeq 10.5$ nm, corresponding to $R_g \simeq 18$ nm is observed, in good agreement with the value of $R_{g,z} \simeq 20$ expected from figure 5. Above the overlap concentration, our data give a power law of ξ [nm] $\simeq 75c^{-0.77}$, where c is in grams per

litres of solution and the exponent has been forced to the theoretical value in good solvents. The scaling model expects a cross-over between $\xi \propto c^{-0.77}$ to $\xi \propto c^{-1}$ at $c \simeq c^{**}$. Our results are not consistent with this behaviour at least up to 400 g/L, which should be well into the concentrated region. The correlation length becomes smaller than the Kuhn length for $c \gtrsim 80$ g/L. This feature is observed also for other neutral polymers as noted by Graessley.[74, 75] When the Kuhn segment exceeds the end-to-end size of a correlation blob, a scaling of $\xi \simeq (bc)^{-1/2}$ is expected. However, the correlation length measured by Eq. 2 measures a lengthscale smaller than the end-to-end distance of a correlation blob[76] and the crossover to the $\xi \simeq (bc)^{-1/2}$ is therefore expected to occur only when ξ_{OZ} is much smaller than l_K , a regime which is likely only applies to the two highest concentrations measured.

In the semidilute regime the osmotic pressure is expected to be approximately k_BT per contact between chains. The number density of binary contacts is of the order of the number density of correlation blobs.[38, 77] An osmotic correlation length (ξ_{Π}) can be defined as:[38, 74]

$$\xi_{\Pi} = \left(\frac{k_B T}{\Pi}\right)^{1/3} \tag{15}$$

The concentration dependence of ξ_{Π} is shown in figure 9a. Values of the ξ_{Π} are calculated from the osmotic pressure reported here and from various literature sources. The osmotic correlation length is seen to be larger than the static one, in agreement with earlier studies on flexible polymer solutions.[74, 75, 78, 79]. Huang and Witten found $\xi_{\Pi}/\xi_{OZ} \simeq 3.81$ and 2.97 for polystyrene in good and θ solvent respectively, in agreement with their theoretical model.[78] The ratio ξ_{Π}/ξ_{OZ} is plotted as a function of concentration in figure 9b for pullulan, where individual ξ_{Π} measurements and ξ_{OZ} from the best fit power-law are used. The values found here for pullulan close to those observed for polystyrene in θ solvent despite water being a thermodynamically good solvent for pullulan.

5 Conclusions

In dilute solution, the intrinsic viscosity, diffusion coefficient, and radius of gyration of pullulan are consistent with those of a flexible neutral polymer. The chain is characterised by a Kuhn segment of about 2.6 nm and a thermal blob comprising roughly 430 glucose units with an end-to-end distance of 20 nm.

Scaling analysis of viscosity, scattering, and osmotic pressure identifies distinct concentration regimes. The dilute–semidilute crossover obtained from viscosity and scattering coincides, but the semidilute–concentrated transition inferred from viscosity ($c^{**} \simeq 20$ g/L) occurs at much lower concentrations than that obtained from osmotic pressure ($\simeq 100$ g/L), while the static correlation length retains good-solvent scaling up to at least 400 g/L. These discrepancies imply that the screening of excluded-volume and hydrodynamic interactions may display different concentration dependences. However, the near-constant ratio $\xi_{\Pi}/\xi_{\rm OZ} \simeq 2.5$, similar to that observed for flexible synthetic polymers in θ solvents, suggests a common underlying mechanism of thermodynamic and structural screening among flexible neutral polymers.

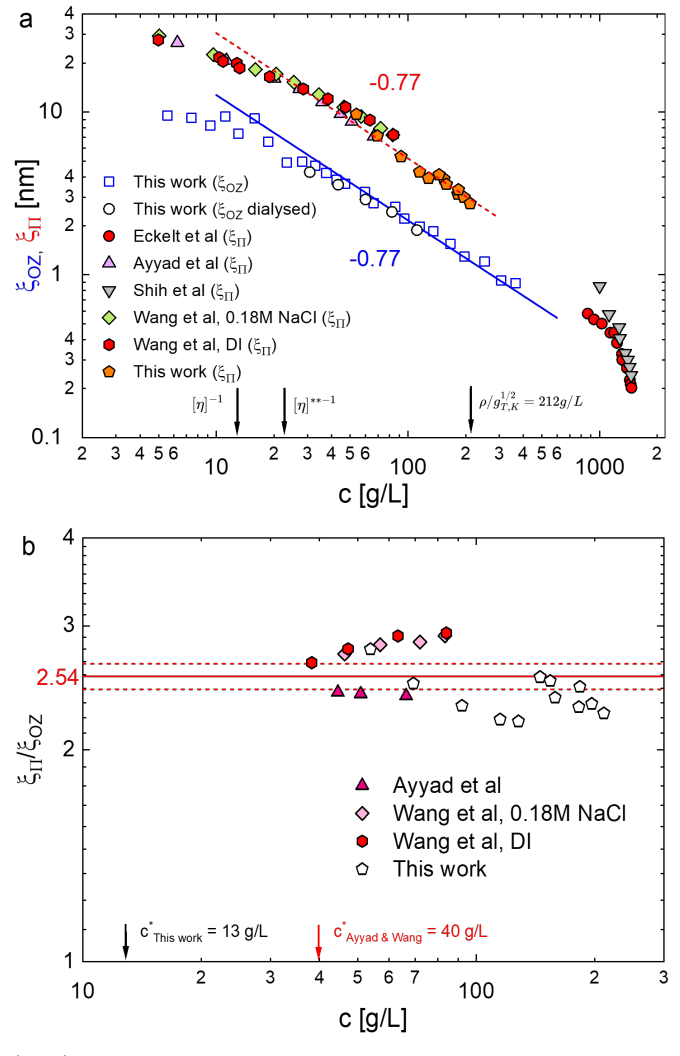


Fig. 9 (a) Static (ξ_{OZ}) correlation length of pullulan in aqueous solution as a function of polymer concentration are shown as blue symbols. The values of c^* and c^{**} estimated as $[\eta]^{-1}$ and $[\eta]^{**-1}$ respectively. The full line is the scaling prediction for semidilute polymers in good solvent $(c < c^{**})$. Filled symbols are the osmotic correlation length calculated from the data in figure 8 and Eq. 15. (b) The ratios of the osmotic and Ornstein-Zernike correlation lengths ξ_{Π}/ξ_{OZ} are plotted as a function of concentration above overlap concentration c^* . The ratios are calculated based on the ξ_{Π} data and the power-law fit for ξ_{OZ} shown in figure 9a. No SAXS measurements were performed above 400 g/L because of the high viscosity of the solutions.

Acknowledgements

We thank the SPring-8 synchrotron facility for SAXS and beamtime (proposal numbers: 2024A1203, 2025A1060 at beamline BL40B2) and Dr. Noboru Ohta and Dr. Albert Mufundirwa for their assistance with the SAXS experiments. The SANS experiment was carried out by the JRR-3 general user program managed by the Institute for Solid State Physics, University of Tokyo (proposal ID: 24813). We thank Dr. Mayumi

for his technical assistance with the SANS experiment. We thank the X-ray Crystal-lography core facility, Penn State Huck Institutes of the Life Sciences and Dr. Neela Yennawar for assistance with the SEC-MALS experiments (NIH grant S10 OD030490). We are grateful to Hayashibra (Okayama, Japan) for donating the pullulan sample. We also thank Dr. Nairiti Sinha (PSU) for access to the freeze drying equipment.

Compliance with Ethical Standards

The authors declare no conflict of interest.

References

- [1] Brant, D.A., Burton, B.A.: The configurational statistics of pullulan and some related glucans, pp. 81–99. ACS Symposium Series, vol 130 (1981)
- [2] Yang, J., Sato, T.: Conformation of pullulan in aqueous solution studied by small-angle x-ray scattering. Polymers **12**(6), 1266 (2020)
- [3] Liu, J.H.-Y., Brameld, K.A., Brant, D.A., Goddard III, W.A.: Conformational analysis of aqueous pullulan oligomers: an effective computational approach. Polymer 43(2), 509–516 (2002)
- [4] Jaud, S., Tobias, D.J., Brant, D.A.: Molecular dynamics simulations of aqueous pullulan oligomers. Biomacromolecules **6**(3), 1239–1251 (2005)
- [5] Liu, J.H.-Y., Brant, D.A., Kitamura, S., Kajiwara, K., Mimura, M.: Equilibrium spatial distribution of aqueous pullulan: Small-angle x-ray scattering and realistic computer modeling. Macromolecules 32(25), 8611–8620 (1999)
- [6] Lopez, C.G., Rogers, S.E., Colby, R.H., Graham, P., Cabral, J.T.: Structure of sodium carboxymethyl cellulose aqueous solutions: A sans and rheology study. Journal of Polymer Science Part B: Polymer Physics 53(7), 492–501 (2015)
- [7] Agrawal, S., Budhwani, D., Gurjar, P., Telange, D., Lambole, V.: Pullulan based derivatives: Synthesis, enhanced physicochemical properties, and applications. Drug delivery **29**(1), 3328–3339 (2022)
- [8] Mishra, B., Mohanta, Y.K., Varjani, S., Mandal, S.K., Lakshmayya, N., Chaturvedi, P., Awasthi, M.K., Zhang, Z., Sindhu, R., Binod, P., et al.: A critical review on valorization of food processing wastes and by-products for pullulan production. Journal of Food Science and Technology 60(8), 2121–2131 (2023)
- [9] Aquinas, N., Chithra, C., Bhat, M.R.: Progress in bioproduction, characterization and applications of pullulan: A review. Polymer Bulletin **81**(14), 12347–12382 (2024)

- [10] Kaith, A., Garg, U., Jain, N., Pandey, M., Kaul, S., Gorain, B., Amin, M.C.I.M.: Pullulan as a sustained release carrier for ocular drug delivery: a review. International Journal of Biological Macromolecules, 143146 (2025)
- [11] Song, Z., Sun, J., Williams, G.R., Liao, X., Xiao, Z., Tang, Y., Zhang, W., Chen, Y., Liu, Y.: Glucan-based biomaterials and their applications in the biomedical field. International Journal of Biological Macromolecules, 144940 (2025)
- [12] Gao, W., Liu, Y., Wu, S.: Properties of pullulan and its effects on starch gelatinization, retrogradation, and protein interaction: A review. Food Chemistry, 144337 (2025)
- [13] Pullulan as a sustainable biopolymer for versatile applications: A review. Materials Today Communications **36**, 106477 (2023)
- [14] Cruz-Santos, M.M., Antunes, F.A.F., Arruda, G.L., Shibukawa, V.P., Prado, C.A., Ortiz-Silos, N., Castro-Alonso, M.J., Marcelino, P.R.F., Santos, J.C.: Production and applications of pullulan from lignocellulosic biomass: Challenges and perspectives. Bioresource Technology 385, 129460 (2023)
- [15] Teixeira, M.O., Marinho, E., Silva, C., Antunes, J.C., Felgueiras, H.P.: Pullulan hydrogels as drug release platforms in biomedicine. Journal of Drug Delivery Science and Technology 89, 105066 (2023)
- [16] Rai, M., Wypij, M., Ingle, A.P., Trzcińska-Wencel, J., Golińska, P.: Emerging trends in pullulan-based antimicrobial systems for various applications. International journal of molecular sciences 22(24), 13596 (2021)
- [17] Thangavel, P., Vilvanathan, S.P., Kuttalam, I., Lonchin, S.: Topical administration of pullulan gel accelerates skin tissue regeneration by enhancing collagen synthesis and wound contraction in rats. International journal of biological macromolecules 149, 395–403 (2020)
- [18] Laksee, S., Sansanaphongpricha, K., Puthong, S., Sangphech, N., Palaga, T., Muangsin, N.: New organic/inorganic nanohybrids of targeted pullulan derivative/gold nanoparticles for effective drug delivery systems. International journal of biological macromolecules 162, 561–577 (2020)
- [19] Zheng, W., Zhang, Z., Li, Y., Wang, L., Fu, F., Diao, H., Liu, X.: A novel pullulan oxidation approach to preparing a shape memory sponge with rapid reaction capability for massive hemorrhage. Chemical Engineering Journal 447, 137482 (2022)
- [20] Ghimici, L., Nafureanu, M.M., Constantin, M.: Cationic pullulan derivatives based flocculants for removal of some metal oxides from simulated wastewater. International Journal of Molecular Sciences **24**(5), 4383 (2023)

- [21] Heo, S., Hwang, H.S., Jeong, Y., Na, K.: Skin protection efficacy from uv irradiation and skin penetration property of polysaccharide-benzophenone conjugates as a sunscreen agent. Carbohydrate polymers **195**, 534–541 (2018)
- [22] Roy, S., Priyadarshi, R., Rhim, J.-W.: Development of multifunctional pullulan/chitosan-based composite films reinforced with zno nanoparticles and propolis for meat packaging applications. Foods **10**(11), 2789 (2021)
- [23] Kato, T., Katsuki, T., Takahashi, A.: Static and dynamic solution properties of pullulan in a dilute solution. Macromolecules **17**(9), 1726–1730 (1984)
- [24] Kawahara, K., Ohta, K., Miyamoto, H., Nakamura, S.: Preparation and solution properties of pullulan fractions as standard samples for water-soluble polymers. Carbohydrate polymers 4(5), 335–356 (1984)
- [25] Nishinari, K., Kohyama, K., Williams, P., Phillips, G., Burchard, W., Ogino, K.: Solution properties of pullulan. Macromolecules **24**(20), 5590–5593 (1991)
- [26] Saito, M.: Wormlike chain parameters of cellulose and cellulose derivatives. Polymer Journal **15**(3), 213–223 (1983)
- [27] Lopez, C.G., Voleske, L., Richtering, W.: Scaling laws of entangled polysaccharides. Carbohydrate polymers **234**, 115886 (2020)
- [28] Kamide, K., Saito, M., Suzuki, H.: Persistence length of cellulose and cellulose derivatives in solution. Die Makromolekulare Chemie, Rapid Communications 4(1), 33–39 (1983)
- [29] Gupta, A., Cotton, J., Marchal, E., Burchard, W., Benoit, H.: Persistence length of cellulose tricarbanilate by small-angle neutron scattering. Polymer 17(5), 363– 366 (1976)
- [30] Lopez, C.G.: Entanglement of semiflexible polyelectrolytes: Crossover concentrations and entanglement density of sodium carboxymethyl cellulose. J. Rheol. 64(1), 191–204 (2020)
- [31] Burchard, W.: Light scattering from polysaccharides. Polysaccharides: Structural diversity and functional versatility 2 (2005)
- [32] Lazaridou, A., Biliaderis, C.G., Kontogiorgos, V.: Molecular weight effects on solution rheology of pullulan and mechanical properties of its films. Carbohydrate Polymers **52**(2), 151–166 (2003)
- [33] Hasegawa, H., Nohara, Y., Saiki, E., Shikata, T.: Onset of entanglement in aqueous solutions of pullulan with narrow molar mass distributions. ACS Applied Polymer Materials 3(8), 4062–4069 (2021)

- [34] Hemar, Y., Pinder, D.: Dws microrheology of a linear polysaccharide. Biomacromolecules **7**(3), 674–676 (2006)
- [35] Hu, H., Takada, A., Takahashi, Y.: Intrinsic viscosity of pullulan in ionic liquid solutions studied by rheometry **42**(3) (2014)
- [36] Hao, H., Takahashi, Y.: Dynamic viscoelastic properties of dilute pullulan ionic liquids solutions 45(3), 133–138 (2017)
- [37] Horinaka, J.-i., Okuda, A., Yasuda, R., Takigawa, T.: Molecular weight between entanglements for linear d-glucans. Colloid and Polymer Science 290, 1793–1797 (2012)
- [38] Rubinstein, M., Colby, R.H.: Polymer physics Oxford university press (2003)
- [39] Graessley, W.W.: Polymer chain dimensions and the dependence of viscoelastic properties on concentration, molecular weight and solvent power. Polymer **21**(3), 258–262 (1980)
- [40] Rhim, J.-W.: Characteristics of pullulan-based edible films. Food Science and Biotechnology **12**(2), 161–165 (2003)
- [41] Cohen, J., Priel, Z., Rabin, Y.: Viscosity of dilute polyelectrolyte solutions. The Journal of chemical physics 88(11), 7111–7116 (1988)
- [42] Shibayama, M., Nagao, M., Okabe, S., Karino, T.: Evaluation of incoherent neutron scattering from softmatter. Journal of the Physical Society of Japan 74(10), 2728–2736 (2005)
- [43] Low molar mass oligosaccharides and/or salt do not influence the osmotic pressure measured by membrane osmometry because they can diffuse through the membrane
- [44] Orthaber, D., Bergmann, A., Glatter, O.: Saxs experiments on absolute scale with kratky systems using water as a secondary standard. Applied Crystallography 33(2), 218–225 (2000)
- [45] Lopez, C.G., Matsumoto, A., Shen, A.Q.: Dilute polyelectrolyte solutions: recent progress and open questions. Soft Matter **20**(12), 2635–2687 (2024)
- [46] Pavlov, G.M., Korneeva, E.V., Yevlampieva, N.P.: Hydrodynamic characteristics and equilibrium rigidity of pullulan molecules. International Journal of Biological Macromolecules 16(6), 318–323 (1994)
- [47] Kato, T., Okamoto, T., Tokuya, T., Takahashi, A.: Solution properties and chain flexibility of pullulan in aqueous solution. Biopolymers: Original Research on Biomolecules 21(8), 1623–1633 (1982)

- [48] Roger, P., Axelos, M.A., Colonna, P.: Sec- malls and sans studies applied to solution behavior of linear α -glucans. Macromolecules **33**(7), 2446–2455 (2000)
- [49] Watanabe, Y., Inoko, Y.: Further application of size-exclusion chromatography combined with small-angle x-ray scattering optics for characterization of biological macromolecules. Analytical and bioanalytical chemistry **399**(4), 1449–1453 (2011)
- [50] Buliga, G.S., Brant, D.A.: Temperature and molecular weight dependence of the unperturbed dimensions of aqueous pullulan. International Journal of Biological Macromolecules **9**(2), 71–76 (1987)
- [51] Wittgren, B., Wahlund, K.-G.: Fast molecular mass and size characterization of polysaccharides using asymmetrical flow field-flow fractionation-multiangle light scattering. Journal of Chromatography A **760**(2), 205–218 (1997)
- [52] Fixman, M.: Polymer dynamics: Non-newtonian intrinsic viscosity. The Journal of Chemical Physics 45(3), 793–803 (1966)
- [53] Yanaki, T., Yamaguchi, M.: Shear-rate dependence of the intrinsic viscosity of sodium hyaluronate in 0.2 m sodium chloride solution. Chemical and pharmaceutical bulletin 42(8), 1651–1654 (1994)
- [54] Lohmander, U., Strömberg, R.: Non-newtonian flow of dilute sodium carboxymethyl cellulose solutions at different ionic strengths and of dilute solutions of cellulose nitrate and polystyrene in moderately viscous solvents studied by capillary viscometry experimental results. Die Makromolekulare Chemie: Macromolecular Chemistry and Physics 72(1), 143–158 (1964)
- [55] Davis, R.M.: Analysis of dilute solutions of (carboxymethyl) cellulose with the electrostatic wormlike chain theory. Macromolecules **24**(5), 1149–1155 (1991)
- [56] Stanković, R., Ilić, L., Nordmeier, E., Jovanović, S., Lechner, M.: Dilute solution properties of pullulan by dynamic light scattering. Polymer Bulletin 27, 337–344 (1991)
- [57] Nordmeier, E.: Static and dynamic light-scattering solution behavior of pullulan and dextran in comparison. The Journal of physical chemistry **97**(21), 5770–5785 (1993)
- [58] Viel, S., Capitani, D., Mannina, L., Segre, A.: Diffusion-ordered nmr spectroscopy: a versatile tool for the molecular weight determination of uncharged polysaccharides. Biomacromolecules 4(6), 1843–1847 (2003)
- [59] Norisuye, T.: Semiflexible polymers in dilute solution. Progress in polymer science 18(3), 543–584 (1993)

- [60] Yamakawa, H., Yoshizaki, T.: Effects of fluctuating hydrodynamic interaction on the hydrodynamic-radius expansion factor of polymer chains. Macromolecules 28(10), 3604–3608 (1995)
- [61] Barrett, A.: Investigation of moments of intrachain distances in linear polymers. Macromolecules 17(8), 1561–1565 (1984)
- [62] Utomo, N.W., Nazari, B., Parisi, D., Colby, R.H.: Determination of intrinsic viscosity of native cellulose solutions in ionic liquids. Journal of Rheology 64(5), 1063–1073 (2020)
- [63] Castellanos, M.M., Pathak, J.A., Colby, R.H.: Both protein adsorption and aggregation contribute to shear yielding and viscosity increase in protein solutions. Soft Matter **10**(1), 122–131 (2014)
- [64] Colby, R.H., Rubinstein, M.: Two-parameter scaling for polymers in θ solvents. Macromolecules **23**(10), 2753–2757 (1990)
- [65] Colby, R.H., Han, A.: Specific viscosity of polymer solutions with large thermal blobs. Rheologica Acta 62(11), 687–693 (2023)
- [66] Lopez, C.G.: Scaling and entanglement properties of neutral and sulfonated polystyrene. Macromolecules **52**(23), 9409–9415 (2019)
- [67] Eckelt, J., Sugaya, R., Wolf, B.A.: Pullulan and dextran: Uncommon composition dependent flory–huggins interaction parameters of their aqueous solutions. Biomacromolecules **9**(6), 1691–1697 (2008)
- [68] Shih, F., Daigle, K., Champagne, E.: Effect of rice wax on water vapour permeability and sorption properties of edible pullulan films. Food Chemistry **127**(1), 118–121 (2011)
- [69] Ayyad, A.H.: Test of the des cloiseaux law by membrane osmometry on pullulan. Macromolecular rapid communications **22**(8), 652–653 (2001)
- [70] Wang, S., Van Dijk, J., Odijk, T., Smit, J.: Depletion-induced demixing in aqueous protein- polysaccharide solutions. Biomacromolecules **2**(4), 1080–1088 (2001)
- [71] Mylonas, E., Svergun, D.I.: Accuracy of molecular mass determination of proteins in solution by small-angle x-ray scattering. Applied Crystallography **40**(s1), 245–249 (2007)
- [72] Higgins, J.S., Benoit, H.C.: Polymers and Neutron Scattering vol. Oxford University Press, (1998)
- [73] The prefactor of the scaling laws of osmotic pressure π obtained based on the osmotic compressibility shown in figure 8b are larger than those obtained by fitting osmotic pressure data shown in figure 8a directly by a factor of 1.5 and

- 2.7 for semidilute and concentrated regions, respectively.
- [74] Graessley, W.W.: Polymeric Liquids & Networks: Structure and Properties vol. Garland Science, (2003)
- [75] Graessley, W.W.: Scattering by modestly concentrated polymer solutions. Macromolecules **35**(8), 3184–3188 (2002)
- [76] This can be seen from the fact that at $c=c^*$, the end-to-end distance of the correlation blob is of the order of the end-to-end size of the chain, but ξ_{OZ} is approximately $\sqrt{3}$ smaller than the radius of gyration of the chain corresponding to a size $\simeq 4 \times$ smaller than the end-to-end distance of the chain.
- [77] Colby, R.H.: Structure and linear viscoelasticity of flexible polymer solutions: comparison of polyelectrolyte and neutral polymer solutions. Rheologica acta 49, 425–442 (2010)
- [78] Huang, J.-R., Witten, T.A.: Universal ratios of characteristic lengths in semidilute polymer solutions. Macromolecules **35**(27), 10225–10232 (2002)
- [79] Raspaud, E., Lairez, D., Adam, M.: On the number of blobs per entanglement in semidilute and good solvent solution: Melt influence. Macromolecules **28**(4), 927–933 (1995)